Published in final edited form as:
J Am Chem Soc. 2007 October 31; 129(43): 13008–13013. doi:10.1021/ja0722067.

Synthetic Efficiency in Enzyme Mechanisms Involving Carbocations: Aristolochene Synthase

Rudolf K. Allemann[†], **Neil J. Young**[†], **Shuhua Ma**[‡], **Donald G. Truhlar**[‡], and **Jiali Gao**[‡]
School of Chemistry, Cardiff University, Park Place, Cardiff, CF10 3AT, UK and Department of Chemistry and Minnesota Supercomputing Institute, University of Minnesota, 207 Pleasant St SE, Minneapolis, MN 55455−0431, USA

Abstract

An intramolecular proton transfer mechanism has been proposed for the carbocationic cyclization of farnesyl pyrophosphate (FPP) to (+)-aristolochene catalyzed by aristolochene synthase. This novel mechanism, which is based on results obtained by high-level *ab initio* molecular orbital and density functional theory calculations, differs from the previous proposal in the key step of carbocation propagation prior to the formation of the bicyclic carbon skeleton. Previously, germacrene A was proposed to be generated as an intermediate by deprotonation of germacryl cation followed by reprotonation of the C6-C7 double bond to yield eudesmane cation. In the mechanism proposed here the direct intramolecular proton transfer has a computed barrier of about 23 kcal/mol, which is further lowered to 16−20 kcal/mol by aristolochene synthase. An alternative pathway is also possible through a proton shuttle via a pyrophosphate-bound water molecule. The mechanism proposed here is consistent with the observation that germacrene A is not a substrate of aristolochene synthase. Furthermore, the modeled substrate-enzyme complex suggests that Trp 334 and Phe 178 play key roles in positioning the substrate in the reactive orientation in the binding pocket. This is consistent with experimental findings that mutations of either residue lead to pronounced generation of aborted cyclization products.

Introduction

Marine and terrestrial plants, fungi, bacteria and insects generate an enormous variety of sesquiterpenes with a multitude of biological functions. The structural variation of sesquiterpenes arises mainly in the cyclisation step in which the universal acyclic precursor farnesyl pyrophosphate (FPP, **1)** is converted to more than 300 distinct sesquiterpene products through the action of sesquiterpene synthases, many of which share a common protein structure known as the terpenoid fold.[1–3] A common mechanistic feature of sesquiterpene formation is the initial cleavage of the alkyl pyrophosphate bond generating a putative carbocation intermediate prior to the cyclisation reactions. Without the pyrophosphate group, a strong acid would be needed to activate the olefinic substrate.[4–6]

The enzyme aristolochene synthase (AS) from *Penicillium roqueforti* catalyses the bivalent metal-dependent cyclisation of FPP to (+)-aristolochene (**6**), the biochemical precursor of several fungal toxins including the potentially lethal PR-toxin (Scheme 1).[7, 8] The enzyme

E-mail: allemannrk@cf.ac.uk, truhlar@umn.edu, gao@chem.umn.edu.
[†]School of Chemistry
[‡]Department of Chemistry and Minnesota Supercomputing Institute

Supporting Information Available: Pdb files (AS-3-Model.pdb and AS-TS2.pdb) for the models of AS containing germacryl cation (**3**) and TS2 docked to the active site, Tables with the calculated free energy changes and calculated electronic energies, and complete refs. [16] and [20]. This material is available free of charge via the Internet at http://pubs.acs.org.

binds FPP in a quasi-cyclic conformation thereby facilitating attack of C1 in farnesyl cation (**2**) by the C10-C11 double bond to produce germacryl cation (**3**).[9, 10] Proton loss from C12 leads to the production of germacrene A (**4**),[11, 12] which was then postulated to undergo reprotonation of the C6-C7 double bond and a further cyclisation to form the bicyclic eudesmane cation (**5**). Successive 1,2 hydride shift and methyl migration followed by loss of H_{Si} on C8 results in the generation of (+)-aristolochene (**6**).[11]

Although several candidates have been proposed for the acid that reprotonates germacrene A (**4**), including a proton shuttle from the solvent to Tyr 92 in the active site by way of Arg 200, Asp 203, and Lys 206,[10, 12] an unprecedented active site oxonium ion,[13] or the pyrophosphate[14] there is a lack of experimental evidence to support them. The main difficulty of the above mechanism is the regeneration of another cation from **4**, which requires a strong acid.

We report here the results from density functional theory (DFT) calculations in the gas phase on the cyclisation of FPP along with molecular docking and modeling studies in the active site of AS, employing combined quantum mechanical and molecular mechanical (QM/MM) methods. The characterization of the inherent gas-phase reactivity of intermediates and transition states along the reaction pathway from farnesyl-cation (**2**) to eudesmane cation (**5**) provided the standard agent which the effects of the active site of AS could be evaluated with. These calculations reveal an alternative, more economical reaction pathway, in which protonation of the C6-C7 double bond is accomplished by intramolecular proton transfer rather than through the involvement of a general acid.

In the following, we first describe the computational details used in the present study, which is followed by results and discussion. We compare the proposed mechanism with available experimental observations. The paper is concluded with a summary of the major findings of this work.

Methods

Gas-phase calculations

An initial structure for **3** was constructed using the HyperChem software (Hyperchem 7.0, Hypercube, Inc. 1115 NW 4th Street, Gainesville, FL 32601 USA) and this geometry was refined using molecular mechanics and AM1. The structure was then modified using the Molden structure visualization program[15] to produce an approximation of the proposed transition state TS1.

Calculations were performed using Gaussian03, revision D.01[16] and Gaussian03, revision B. 05. A variety of semi-empirical and density functional theory methods were employed, namely AM1, PM3, mPW1PW/6−31+G(d,p) and MPWB1K/6−31+G(d,p). Energy calculations were also made at the MP2/6−31+G(d,p)//MPWB1K/6−31+G(d,p) level. When calculating the free energy of each species the harmonic oscillator approximation was applied. For the lowest energy vibrational modes, the frequencies of all vibrational modes below 100 cm^{-1} were raised to 100 cm^{-1} prior to the free energy calculations as a way to approximately account for anharmonicity.

A transition state search was carried out on the initial geometry and transition state TS1 was calculated. In order to identify transition state precursor **2** the interatomic distance between C1 and C11 was increased by 2 Å and a geometry optimisation performed to find structure **2**.

The structure of **2** obtained using the AM1 method was subjected to a relaxed potential energy surface scan where the reaction coordinate was described as the C1-C11 interatomic distance.

The approximate structure of **3** was optimized. A reaction coordinate based upon a C6 hydrogen atom and C12 was then defined, a transition state search corresponding to the intramolecular proton transfer from C12 to C6 was performed, and transition state TS2 identified. From transition state TS2 it was then possible to calculate the minimum energy geometry of the eudesmane cation **5**.

Enzyme Model

The enzyme-substrate model was constructed by an iterative approach using CHARMM for energy optimization [17] and Insight II (Biosym Technologies Inc. San Diego) for visualization and further structural adjustment. The crystal structure of aristolochene synthase from *Penicillium roqueforti* (PDB code: 1DGP) was used as a starting point.[18] This structure is of the apoenzyme but contains a modeled farnesol molecule. The transition structure for the intramolecular proton transfer (TS2) was kept rigid and used in the docking calculations. The initial results from molecular docking followed closely the results obtained by site-directed mutagenesis, which identified key residues involved in metal ion binding.[13] Then, the carbocation intermediate **3** was used to replace that of the transition state structure. All energy calculations were performed using a combined quantum mechanical and molecular mechanical (QM/MM) potential[19] in which the carbocationic substrate was treated by the semiempirical AM1 model and the rest of the protein and solvent by the CHARMM22 force field[20] for the protein and the TIP3P model for water.[21]

The active site consists of a pyrophosphate binding site mediated by two Mg^{2+} ions, and a farnesyl folding pocket, characterized by both aliphatic and aromatic residues.[18] In our model, the first Mg^{2+} ion is coordinated by a pyrophosphate bridge along with Ser 248 and Glu 252 and two water molecules. Asn 244, which has been described as one of the three residues in the Mg^{2+} binding triads forms a hydrogen-bonding network by donating a hydrogen bond to the P1-phosphate group and by accepting a hydrogen bond from Ser 244.[18] The role of Asn 244 is essential and it is the only residue of the Mg^{2+} binding triads whose single-mutation completely abolishes the enzyme activity.[13] The double roles of the hydrogen-bonding network, coordinating both the pyrophosphate ion and Ser 248, is consistent with experimental observations. The second Mg^{2+} ion is coordinated to the P2-phosphate group, which is exposed to the solvent and is located in the aspartate-rich domain, consisting of Asp 115, Asp 116 and Asp 119.[18] In addition, the charges of the pyrophosphate ion are further compensated by an ion-pair interaction between the P1 phosphate group and Arg 329 and a water molecule.

The enzyme may actually function in the presence of three magnesium ions. X-ray crystal structures have been obtained for the apoenzyme [18, 22] and for the tetrameric AS from *A. terreus* where the active site of one subunit was occupied by a pyrophosphate molecule bound to three Mg-ions.[22] In the latter structure, the third magnesium ion contains four water molecules as ligands, suggesting that it is not tightly associated with the protein. Since the focus in this work was the proton transfer mechanism rather than the metal binding interactions, the present modeling study of the enzymatic reaction provides a reasonable assessment of the proton transfer pathway.

Results and Discussion

In the previously proposed reaction mechanism for the AS-catalyzed conversion of FPP to aristolochene, the high-energy carbocationic intermediate **3** is converted to the neutral germacrene A (5) through proton loss from C12 (Scheme 1). Energy minimisations of **3** revealed that the protons of the C12 and C13 methyl groups could be brought into close proximity to the C6-C7 double bond by rotation of the isopropyl group thereby suggesting an intramolecular proton transfer in **3** to generate **5** (Scheme 1, Figure 1). In such a mechanism, germacrene A is not a reaction intermediate but rather a side product formed by the abstraction

of a proton and quenching of the positive charge on C11 in **3**. From the structure of **3,** optimised by density functional theory, the free energies of the transitions states prior to and following **3** (TS1 and TS2) as well as of **2** and **5** were calculated using the mPW1PW[23] and MPWB1K[24] density functionals and the MPWB1K optimised geometries were used to perform single point energy calculations using second order Møller-Plesset perturbation theory (MP2). To test the performance of computationally less expensive methods, we also compared the results to those obtained using the neglect-of-diatomic overlap methods AM1[25] and PM3.[26]

Overall broad agreement was observed between the results obtained using density functional theory (mPW1PW and MPWB1K), MP2 and semi-empirical methodologies (AM1, PM3) (Table 1, Figure 2). The results generated by AM1 and PM3 methods were remarkably similar to those obtained from the more sophisticated DFT methods, suggesting that it is reasonable to use these methods to examine the effect of the enzyme on the reaction energetics. The conversion of **2** to **3** was slightly endergonic for all methods except MP2, while the intramolecular proton transfer via TS2 was strongly exergonic for all methods (Table 1, Figue 2). The free energy of TS2 is approximately 23 to 26 kcal/mol higher than that of **3**, whereas it was found that **7**, where the carbocation is located on C7 is not an intermediate before cyclisation to **5**. The distances d_1 between C2 and C7 in **3** (3.1 and 2.92 Å for DFT) and in TS2 (3.02 and 2.98 Å) were similar (Table 2). In eudesmane cation (**5**), however, this distance was shortened to 1.66 or 1.64 Å indicating the formation of a sigma-bond between C2 and C7. The migrating proton was approximately equidistant between C12 and C6 in TS2 at all levels of theory (Figure 1, Table 2). The angle α between C6, the transferring proton and C12 was between 151 and 161° suggesting that the stereochemistry of the transfer does not require a large distortion from linearity (Table 2). The absence of an intermediate with a positive charge on C7 suggests that the formation of the σ-bond between C2 and C7 is concerted with the intramolecular proton transfer.

In the Marcus theory of proton transfer,[27] the free energy of activation is partitioned into that associated with the bond rearrangement and another part which represents the motion necessary to reach the configuration or orientation in which the rearrangement can take place. An efficient proton transfer process requires not only a low intrinsic barrier but also that the free energy required for the pre-rearrangement not be large. The reaction energy profile for the formation of **3** indicates a cyclisation-induced pre-organisation of the molecular structure in that the initial cyclisation step forces the terminal isopropyl group to orient the C12 methyl group towards the C5-C6 double bond followed by a further rotation of about 40° around the C10-C11 single bond during the formation of the transition state. To evaluate the energetic cost of this rotation, the potential energy as a function of the dihedral angle β in **3** was calculated (Figure 3 and Table 2). The energy of the structure, **3***, at which β is the same as that in TS2 is between 0.02 (for MPWN1K) and 1.9 kcal /mol (for AM1) higher than that of **3**, indicating that the rotation around the C10-C11 bond contributed only a small amount to the energetic cost of the conversion of **3** to TS2 (Figure 3 and Table 2). Thus, the major contribution to the energy barrier separating **3** and **5** is associated with the transfer of the proton from C12 to C6.

To illustrate that intramolecular proton transfer is a plausible mechanism in the active site of AS, we have generated a model of the enzyme-substrate complex. The enzyme-substrate model was constructed based on the results of site-directed mutagenesis experiments, which revealed different amounts of aberrant cyclisation products in various mutant enzymes.[9, 12, 13] The active site consists of a pyrophosphate binding site, facilitated by two Mg^{2+} ions, and a farnesyl folding pocket, characterized by aliphatic and aromatic residues (Figure 4).[18] In our model, the first Mg^{2+} ion is coordinated by a pyrophosphate bridge along with Ser 248 and Glu 252 and two water molecules. Asn 244, which has been described as one of the three residues in the Mg^{2+} binding triads forms a hydrogen-bonding network by donating a hydrogen bond to

the P1-phosphate group and by accepting a hydrogen bond from Ser 248. The role of Asn 244 is essential and it is the only residue of the Mg^{2+} binding triads whose single-mutation completely abolishes the enzyme activity.[13] The double roles of the hydrogen bonding network, coordinating the positions of both the pyrophosphate ion and Ser 248, is consistent with the experimental observation. The second Mg^{2+} ion is coordinated to the P2-phosphate group, which is exposed to the solvent and is located in the aspartate-rich domain, consisting of Asp 115, Asp 116 and Asp 119.[13] In addition, the charges of the pyrophosphate ion are further compensated by an ion-pair interaction between the P1 phosphate group and Arg 329 and a water molecule (*vide infra*).

The farnesyl-binding pocket was modelled by using the cyclisation intermediate **3** as the template. Consistent with experiments that revealed inversion of configuration at C1,[11] we placed the C1 carbon closer to the pyrophosphate ion and the C10 carbon away from the pyrophosphate group (Figure 4). Other key structural features are that Trp 334 is about 3.5 Å from the C4 atom while, on the opposite side, Phe 178 is about 3.5 Å from the putative isopropyl cation. The latter residue is predicted to be particularly important for restraining rotation about the C10-C11 single bond of **3**, resulting in specific proton loss from C12 in product formation.[11] The only polar residue in the farnesyl binding pocket is Tyr 92, which is located in close proximity to the C6-C7 double bond. The water molecule that is hydrogen-bonded to the phosphate group is situated roughly between the phosphate group and the center of **3**. In principle, this water could act as a proton shuttle for transfer from the C12 methyl group to the C6-C7 double bond via a water bridge (*vide infra*).

We used this model of the enzyme-substrate complex to examine the effects of the enzyme on the relative energies along the cyclisation cascade and evaluated the relative stabilization energies for **3** and TS2 within the active site using the combined QM/MM method.[19] AM1 and CHARMM were used for the QM and MM components, respectively. We found that TS2 is stabilised by 5 to 7 kcal/mol in the enzyme relative to the gas phase barrier (Table 3) indicating that the enzyme environment is capable of further reducing the already reasonable barrier height for the intramolecular proton transfer pathway. An environmental effect of this magnitude would bring the overall barrier height to a value of about 16 to 20 kcal/mol which is a reasonable range compared with the experimental rate constant.[7, 28]

The results presented here suggest an energetically feasible pathway for the production of **5** from **3** that does not go through the intermediate germacrene A. Rather an intramolecular proton transfer from C12 to C6 in **3** occurs which bypasses **4**. The small amount of germacrene A produced by the wild type enzyme is the result of proton loss from C12 in **3** to generate the isopropylidene group of **4**. The mechanism proposed here is supported by the observation that **4** is not a substrate of AS.[12]

It is also consistent with mutagenesis experiments. When Tyr 92 was replaced with Phe significant amounts of aristolochene were still produced albeit with reduced catalytic efficiency,[10, 12, 13] suggesting that the presence of Tyr 92 was not mandatory for the synthesis of **6**. The mechanism proposed here suggests that Tyr 92 provides electrostatic stabilization of the development of the transient C7 cation as a result of the intramolecular proton transfer and is consistent with the production of **5** by the mutant protein.

Mutagenesis experiments had shown that the Trp 334 in AS was necessary for the stabilization of eudesmane cation.[29] When Val or Leu substituted the aromatic residue the almost exclusive production of germacrene A was observed. However, the catalytic efficiencies of the mutants were reduced by almost 4 orders of magnitude mainly as a consequence of significantly smaller turnover numbers. In our active site model, Trp 334 together with Phe 178 provide key anchoring roles that restrict the folding and movement of the substrate. Mutations of Trp 334

to smaller residues relieve such restraints, resulting in configurations more suitable for proton abstraction from C12 in the intermediate **3**, which has a smaller free energy barrier than the intramolecular proton transfer. In the same vein, the results presented here would predict that mutations of Phe 178 to smaller residues such as alanine or valine would lead to an increase in aborted products. This was indeed found in the mutant AS-F178V where in addition to substantially increased levels of germacrene A, α- and β-selinenes as well as selina-4,11-diene and (*E*,*E*)-α- and (*E*)-β-farnesenes were observed.[30] On the other hand, only minor changes in the product distribution resulted when tyrosine replaced phenylalanine. The intramolecular proton transfer mechanism is consistent with these experiments, whereas it cannot easily be explained by previous proposals.

In a previously published study, the isotope labeled substrates 12,12,12-[$^2H_3$]-FPP and 13,13,13-[$^2H_3$]-FPP were incubated with AS from *Asperillus terreus* to determine the stereochemistry of proton loss.[11] Analysis of the products by ^{2}H- NMR revealed that deuteron abstraction occurred at C12 in agreement with the intramolecular proton transfer mechanism proposed here. Unfortunately, only the methyl and vinyl region of the spectrum were reported in detail while the region of the ^{2}H-NMR spectrum around1.5 ppm, where the signals from deuterons on C6 would be expected, was not described. However, the potential absence of deuterium incorporation at C6 would not exclude a transfer of the label from C12 as proposed here, but may simply suggest an indirect mechanism in which the transfer occurs by way of an active site general acid such as a bound water molecule or the pyrophosphate group.[22] Such a water molecule has been identified in the model of the transition state (TS2) in the active site of AS (Figure 4).

Concluding Remarks

The computational results presented here provide a thermodynamically feasible reaction mechanism for the conversion of farnesyl to eudesmane cation during AS catalysis that, to the best of our knowledge, is in agreement with all available experimental data. There is precedent in other enzymatic terpenoid cyclisations for such intramolecular proton transfer that avoids the quenching and regeneration of high-energy carbocationic intermediates.[31–33] Hence the highly economical mechanism for aristolochene synthase proposed here might be a general reflection of the high synthetic efficiency in the large family of terpenoid synthases.

Supplementary Material

Refer to Web version on PubMed Central for supplementary material.

Acknowledgment

The financial support of the Biotechnology and Biological Science Research Council (RKA, NJY) is gratefully acknowledged. This work was also supported by the National Institutes of Health (GM46736) (JG). The authors would like to thank Dr James Platts for his guidance during the initial stages of this work.

REFERENCES

1. Cane DE. Chem. Rev 1990;90:1089–1103.
2. Lesburg CA, Caruthers JM, Paschall CM, Christianson DW. Curr. Opin. Struct. Biol 1998;8:695–703. [PubMed: 9914250]
3. Glasby, JS. Encyclopedia of Terpenoids. Wiley; Chichester: 1982.
4. Rajamani R, Gao J. Am. Chem. Soc 2003;125:12768–12781.
5. Wendt KU, Schulz GE, Corey EJ, Liu DR. Angew. Chem. Int. Ed 2000;39:2812.
6. Corey EJ, Cheng HM, Baker CH, Matsuda SPT, Li D, Song XL. J. Am. Chem. Soc 1997;119:1289–1296.

7. Hohn TM, Plattner RD. A. Biochem. & Biophys 1989;272:137–143.
8. Proctor RH, Hohn TM. Aristolochene synthase. J. Biol. Chem 1993;268:4543–4548. [PubMed: 8440737]
9. Deligeorgopoulou A, Allemann RK. Biochemistry 2003;42:7741–7747. [PubMed: 12820883]
10. Calvert MJ, Taylor SE, Allemann RK. Chem. Commun 2002;20:2384–2385.
11. Cane DE, Prabhakaran PC, Oliver JS, Mc Ilwaine DB. J. Am. Chem. Soc 1990;112:3209–3210.
12. Calvert MJ, Ashton PR, Allemann RK. J. Am. Chem. Soc 2002;124:11636–11641. [PubMed: 12296728]
13. Felicetti B, Cane DE. J. Am. Chem. Soc 2004;126:7212–7221. [PubMed: 15186158]
14. Shishova E,Y, Di Constanzo L, Cane David E, Christianson David W. Biochemistry 2007;46:1941–1951. [PubMed: 17261032]
15. Schaftenaar G, Noordik JH. Molden. J. Comp. Mol Design 2000;14:123–134.
16. Frisch MJ, et al. Gaussian 03, Revision B.03/D.05.
17. Brooks BR, Bruccoleri RE, Olafson BD, States DJ, Swaminathan S, Karplus M. J. Comp. Chem 1983;4:187–217.
18. Caruthers JM, Kang I, Rynkiewicz MJ, Cane DE, Christianson DW. J. Biol. Chem 2000;275:25533–25539. [PubMed: 10825154]
19. Gao J. Rev. Comp. Chem 1995;7:119–185.
20. MacKerell AD, et al. Phys. Chem. B 1998;102:3586–3616.
21. Jorgensen WL, Chandrasekhar J, Madura JD, Impey RW, Klein ML. J. Chem. Phys 1983;79:926–935.
22. Adamo C, Barone V. J. Chem. Phys 1998;108:664–675.
23. Zhao Y, Truhlar DG. J. Phys. Chem. A 2004;108:6908–6918.
24. Dewar MJS, Zoebisch EG, Healy EF, Stewart JJP. J. Am. Chem. Soc 1985;107:3902–9.
25. Stewart JJP. J. Comp. Chem 1989;10:209–220.
26. Marcus RA. Faraday Symp. Chem. Soc 1975;108:664.
27. Forcat S, Allemann RK. Org. Biomol. Chem 2006;4:2563–2567. [PubMed: 16791319]
28. Deligeorgopoulou A, Taylor SE, Forcat S, Allemann RK. Chem. Commun 2003;17:2162–2163.
29. Forcat S, Allemann RK. Chem. Commun 2004;18:2094–2095.
30. Shishova EY, Di Costanzo L, Cane DE, Christianson DW. Biochemistry 2007;46:1941–1951. [PubMed: 17261032]
31. Williams DC, Carroll BJ, Jin Q, Rithner CD, Lenger SR, Floss HG, Coates RM, Williams RM, Croteau R. Chem. & Biol 2000;7:969–977. [PubMed: 11137819]
32. Ravn MM, Coates RM, Flory JE, Peters RJ, Croteau R. Org. Lett 2000;2:573–576. [PubMed: 10814381]
33. Ravn MM, Coates RM, Jetter R, Croteau RB. Chem. Commun 1998;1:21–22.

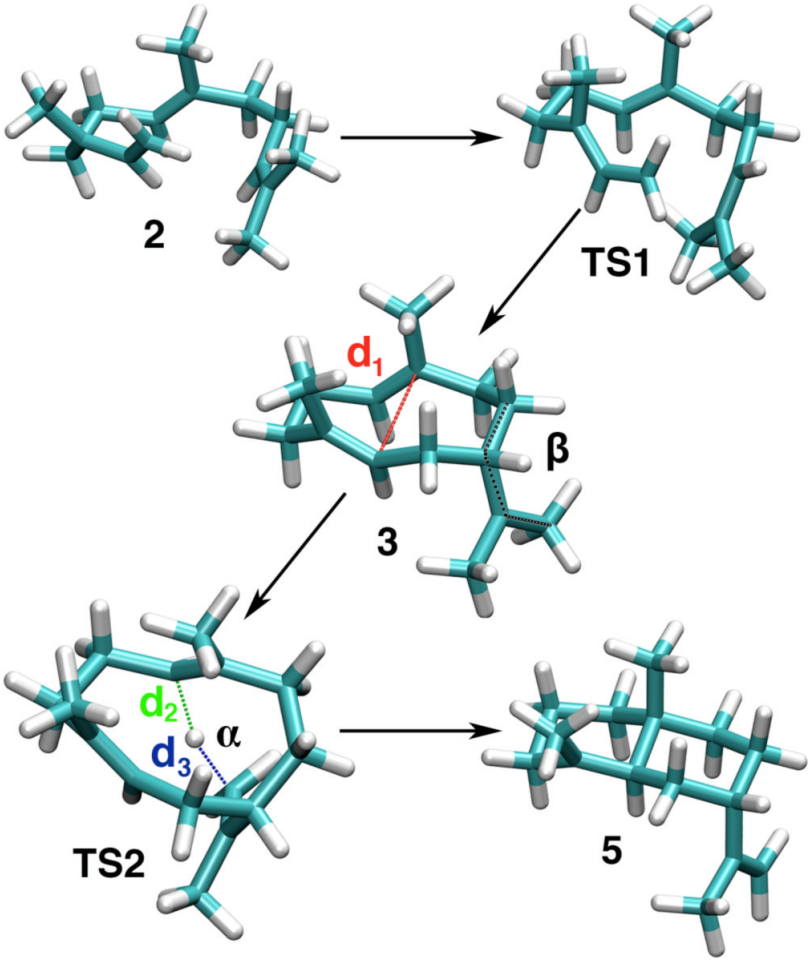

Figure 1.
Structures, reaction intermediates, and transition states for the conversion of farnesyl cation **2** to eudesmane cation **5** as obtained from MPWB1K/6−31+G(d,p) calculations. The values obtained by the calculations for the distances d_1, d_2, d_3 and the angles α and β are listed in Table 1.

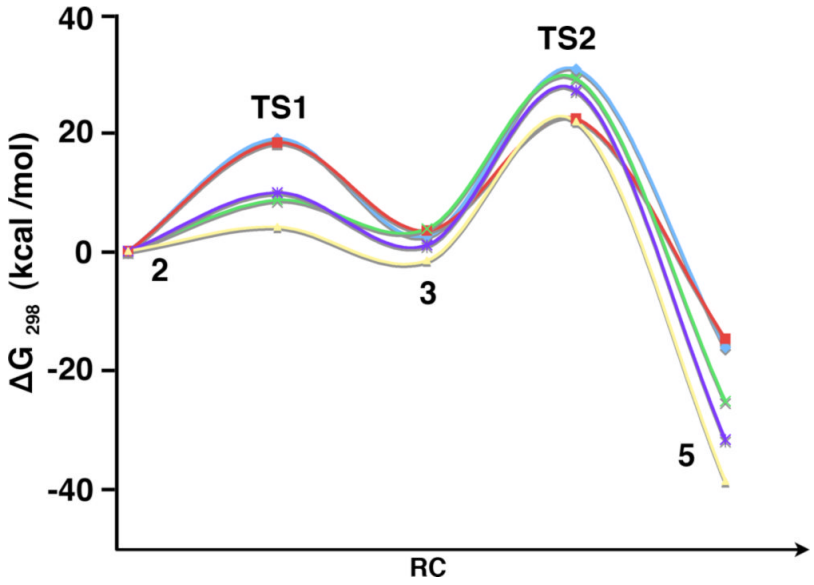

Figure 2.

Free energy diagram for the conversion of farnesyl cation (**2**) to eudesmane cation (**5**) along an arbitrary reaction coordinate. All energies are relative to that of **2**, which was set to 0 kcal / mol. Lines represent the results from AM1 (light blue), PM3 (red), mPW1PW (yellow), MPWB1K (green), and MP2 (purple) calculations. MP2 results are for ΔE at the MP2/6−31 +G(d,p)//MPWB1K/6−31+G(d,p) level.

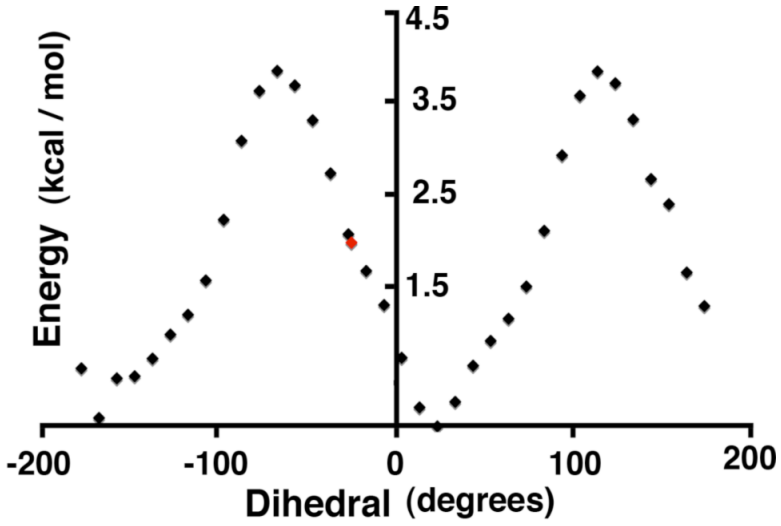

Figure 3.

AM1 energy of germacryl cation (**3**) as a function of the C9, C10, C11 and C12 dihedral angle β. E = 0 kcal / mol corresponds to the value of β in **3**, while the red point indicates the energy of **3** for β in **3***.

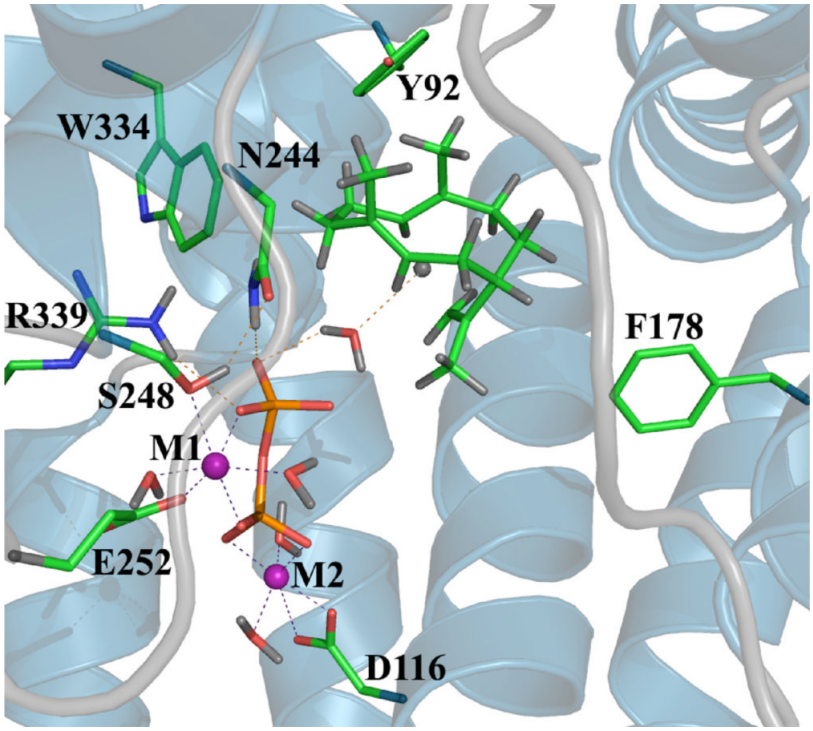

Figure 4.

Sketch of the model of the calculated transition state structure TS2 and of pyrophosphate in the active site of AS.[18] Purple spheres indicate the Mg^{2+} ions. The residues of the Mg^{2+} binding triad as well as Tyr 92, Phe 178, Asn 244, Trp 334 and Arg 339 are indicated. A water molecule bonded to the pyrophosphate group and in close proximity to the transferring proton as well as water molecules involved in metal coordination are indicated.

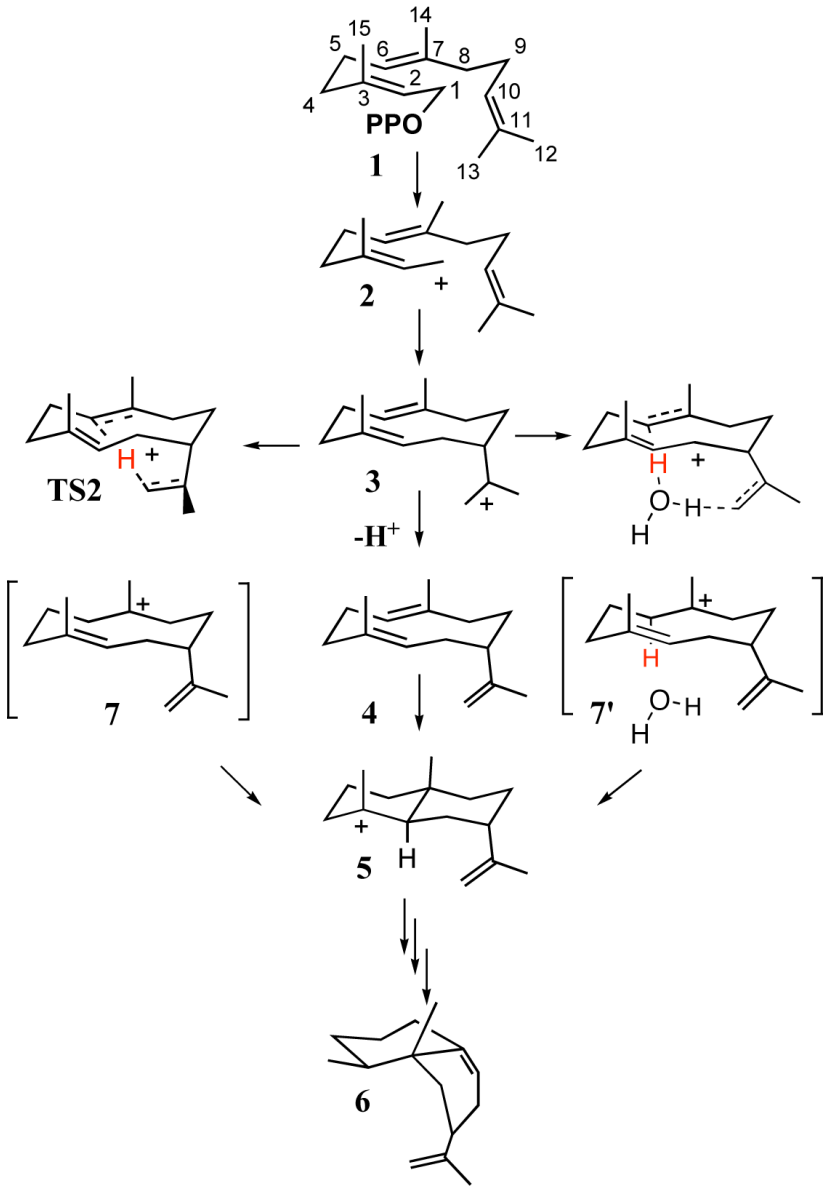

Scheme 1.

Table 1

Free energies, ΔG^{o}_{298}, of reaction intermediates for the conversion of farnesyl cation (**2**) to **5**. All energies are reported relative to the free energy of farnesyl cation (**2**).[a]

	ΔG^{o}_{298} (kcal/mol)				
	2	**TS1**	**3**	**TS2**	**5**
AM1	0	18.9	2.6	30.6	−16.2
PM3	0	18.2	3.5	22.3	−14.7
mPW1PW	0	8.6	3.8	29.0	−25.2
MPWB1K	0	9.9	1.1	27.1	−31.6
MP2[b]	0	4.12	−1.53	21.8	−38.6

[a] The 6−31+G(d,p) basis set is used in all DFT calculations.

[b] Determined by single-point energy calculations using the MPWB1K optimized structures.

Table 2

Distances d_1, d_2, and d_3 the angles α and β for the conversion of **3** to **5**, the dihedral angle β between C9, C10, C11, and C12 in germacryl cation (**3**) and in **3*** (**3** with β as calculated for TS2) (as defined in Figure 1) and the energy barrier for the conversion of **3** to **3***.

	d_1 (Å)			d_2 (Å)	d_3 (Å)	A (deg)	β (deg)		ΔE (3 → 3*) (kcal/mol)
	3	TS2	5		TS2		3	3*	
AM1	2.92	2.99	1.55	1.45	1.45	151	23.0	−25.2	1.9
PM3	3.09	3.03	1.55	1.45	1.45	151	15.9	−29.9	1.5
mPW1PW	3.10	3.02	1.66	1.46	1.44	161	18.4	−19.9	1.0
MPWB1K	3.00	2.98	1.64	1.47	1.46	159	15.9	−18.3	0.02

Table 3

Relative enthalpies between the two structures, computed by the combined QM/MM potential for the substrate species in the gas phase and in the enzyme.[a] The enthalpy of activation, ΔH, is shown as well as the change in enthalpy, ΔΔH, resulting from the interaction with the enzyme and the solvent.

	3 (kcal/mol)	TS2 (kcal/mol)	ΔH (kcal/mol)	ΔΔH (kcal/mol)
$\Delta\Delta H^{o}_{f\,(\text{Gas phase})}$	194.4	221.2	26.8	0
$\Delta H_{qm/mm(\text{Enzyme})}$	−114.5	−95.0	19.5	−7.3
$\Delta H_{qm/mm(\text{Enzyme with active site water})}$	−114.2	−92.2	22.0	−4.8

[a] These values include electronic energy, nuclear repulsion zero point vibrational energy, and thermal vibrational contributions. The vibrational energies were computed with frequencies below 100 wave numbers raised to 100 wave numbers.